THE JOURNAL OF PHYSICAL CHEMISTRY C

Article

pubs.acs.org/JPCC

Sensing the Moving Direction, Position, Size, and Material Type of Nanoparticles with the Two-Photon-Induced Luminescence of a Single Gold Nanorod

Lei Chen,[†] Guang-Can Li,[†] Guang-Yin Liu,[†] Qiao-Feng Dai,[†] Sheng Lan,*[,†] Shao-Long Tie,[‡] and Hai-Dong Deng[§]

[†]Laboratory of Nanophotonic Functional Materials and Devices, School of Information and Optoelectronic Science and Engineering, South China Normal University, Guangzhou 510006, People's Republic of China

[‡]School of Chemistry and Environment, South China Normal University, Guangzhou 510006, People's Republic of China

[§]College of Science, South China Agricultural University, Guangzhou 510642, People's Republic of China

ABSTRACT: We propose a numerical method to evaluate the two-photon-induced luminescence (TPL) of single gold nanorods (GNRs). The validity of this method is confirmed by the $\cos^4 \alpha$ dependence of the TPL of single GNRs on the polarization angle α, which is in good agreement with experimental observations. As comparing with their linear optical properties such as scattering and absorption, the TPL of a single GNR is found to be more sensitive to the change of the surrounding environment. This property is exploited to detect nanoparticles (NPs) approaching the GNR from a far place. By monitoring the evolution of the TPL on the distance between the GNR and a NP, it is possible to extract various information on the NP, including the moving direction, position, size, and material type. For GNRs whose extinction is dominated by absorption, the response and sensitivity are found to depend strongly on their sizes. The detection of the nonlinear optical responses of GNRs may find potential applications in the fields of nanophotonics and biophotonics.

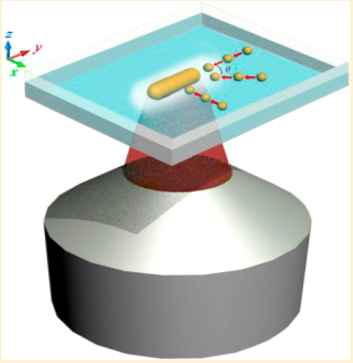

1. INTRODUCTION

Localized surface plasmon polaritons (SPPs) or surface plasmon resonances (SPRs) excited in nanoparticles (NPs) of noble metals have attracted great interest in the past decade due to their potential applications in various fields of nanometer science and technology.[1] Typical examples in which the SPRs of NPs have been successfully utilized include surface enhanced Raman scattering[2−4] and five dimensional optical data storage media.[5−7] In the former case, the significant enhancement in Raman signal of several orders of magnitude was achieved by the local enhancement of electric field on the surfaces of NPs. In the latter case, the strong polarization and wavelength dependence of the longitudinal SPRs (LSPRs) of gold nanorods (GNRs) were exploited to realize the polarization and wavelength multiplexing in optical data storage. As compared to NPs of other shapes, GNRs have received intensive and extensive studies because of the existence of LSPRs, which significantly influence the optical properties of GNRs.[8]

It has been known that there exist two SPRs in GNRs, namely, the transverse SPRs (TSPRs) and LSPRs, which correspond to the collective oscillations of electrons along the short and long axes of GNRs, respectively.[9,10] While the former remains nearly unchanged at ∼530 nm, the latter is quite sensitive to the dielectric environment surrounding GNRs.[11] This unique feature has been employed to fabricate sensors of different types.[12−14] From the experimental point of view, the LSPRs of GNRs can be detected through the measurements of the scattering spectra of GNRs by using dark-field microscopy.[15−17] However, the signal-to-noise ratio in scattering spectra measurements is generally not satisfied for small GNRs whose extinction is dominated by absorption rather than scattering. On the other hand, the line width of the LSPRs of single GNRs, which reflect the homogeneous broadening of the LSPRs, is estimated to be ∼100 meV at room temperature.[16,17] For this reason, it is difficult to accurately determine the shift of LSPRs in most cases because of the broad line width. In practical applications, the difficulties in both the detection of LSPRs and the determination of their shift severely hinder the use of this property in making sensors with high sensitivities.

Apart from their linear optical properties, the nonlinear optical properties of GNRs have become the focus of many studies in recent years.[18−22] Physically, it is anticipated that the detection of the nonlinear optical properties, such as second harmonic generation (SHG)[18,19] and two-photon-induced luminescence (TPL),[20] will offer higher resolution in both the space and frequency domains. In experiments, SHG and TPL have been observed in GNRs of different sizes. Very recently, we demonstrated the existence of a size-dependent competition between SHG and TPL in GNRs.[23] However, a systematic investigation of sensing NPs by detecting the

Received: May 31, 2013
Revised: August 3, 2013
Published: September 5, 2013

nonlinear optical responses of GNRs, which is quite useful in the fields of nanophotonics and biophotonics, is still lacking.

In this article, we propose a numerical method to evaluate the TPL of single GNRs. It is revealed that the TPL of a GNR is quite sensitive to the NPs approaching the GNR. By monitoring the evolution of the TPL with the distance between the GNR and the NP, it is possible to extract various information on the NP, including the moving direction, position, size, and material type.

2. PHYSICAL MODEL AND NUMERICAL METHED

The physical model for the proposed sensor based on a single GNR is schematically depicted in Figure 1. A single GNR

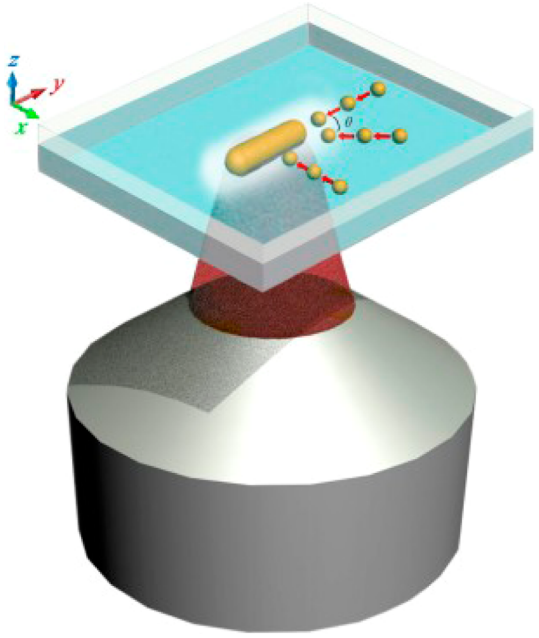

Figure 1. Schematic showing the use of a single GNR to sense moving NPs.

immersed in water is excited with a femtosecond laser light focused by using the objective lens of an inverted microscope. The TPL emitted by the GNR is collected by using the same objective lens and directed to a detector (e.g., a photomultiplier tube (PMT)) connected to the microscope for analysis. Suppose that nanospheres (NSs) made of different materials, such as metals, semiconductors, and dielectrics, approach the GNR from different directions. For simplicity, we consider here NSs made of Au, Si and SiO_2 and moving directions with θ = 0°, 30°, and 90°, where θ denotes the angle between the moving direction of NSs and the long axis of the GNR.

The GNR studied in this paper is a cigar-like GNR composed of a cylinder in the middle and two hemispheres on both sides. The length and diameter of the GNR are chosen to be 45 and 12 nm, corresponding to an aspect ratio of 3.75. The extinction spectrum of the GNR, which is the sum of the absorption and scattering spectra, can be easily calculated by using the discrete dipole approximation (DDA) method.[24,25] The dielectric permittivity for gold and its dispersion relation used in the calculations can be found in ref 26. The refractive index of water was chosen to be 1.33. The simulations were performed on a cubic lattice with a lattice constant of 0.5 nm. For the GNR mentioned above, the total number of dipoles was estimated to be ~33747, giving a dipole density of ~8 nm^{-3}. The same dipole density was also used for the NSs studied in this paper. For the smaller and larger GNRs discussed later, the lattice constant was chosen to be 0.25 and 1.0 nm, respectively.

As shown in Figure 2, the extinction of the GNR is dominated by absorption because of the small size of the GNR.

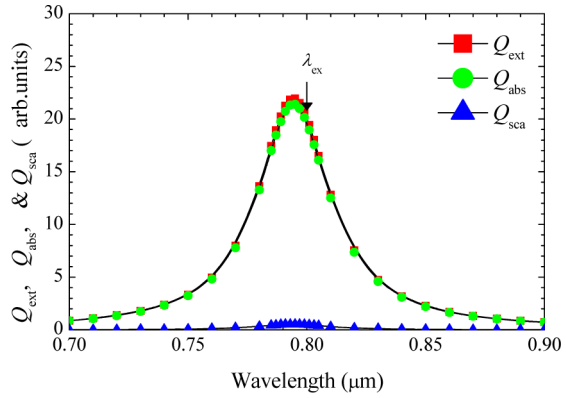

Figure 2. Extinction, absorption and scattering spectra calculated for a cigar-like GNR with a length of 45 nm and a diameter of 12 nm by using the DDA method. Q_{ext}, Q_{abs}, and Q_{sca} represent the excitation, absorption, and scattering efficiencies of the GNR, respectively.

The absorption given in Figure 2 is the linear absorption of the GNR with a peak at 795 nm. The absorption given in this paper is the absorption efficiency, which is defined as the absorption cross section of a NP divided by its effective cross section. In order to evaluate the TPL emitted by the GNR, we need to consider the two-photon absorption (TPA) of the GNR excited by the femtosecond laser light. The wavelength of the femtosecond laser is chosen at 800 nm, which is slightly detuned from the LSPR of the GNR. It will be shown later that this choice makes it easier to discriminate small NPs from large ones based on the change in the TPL of the GNR.

Previously, Xu and Webb investigated the two-photon excitation of fluorophores and derived the TPA of a sample containing uniformly distributed dye molecules as follows:[27]

$$N_{abs} = C\delta I_0(t) \int_V S^2(r)\, dV \quad (1)$$

Here, N_{abs} is the number of photons absorbed per unit time, C is the concentration of dye molecules, δ is the TPA cross section, $S(r)$ and $I(t)$ describe the spatial and temporal distributions of the incident light. In our case, the excitation light is considered to be a plane wave because the excitation spot, which is about 1 μm in diameter when a 100× objective lens is used, is much larger than the size of the GNR. Physically, the TPL of the GNR is determined not only by the TPA at the excitation wavelength (λ_{ex}), but also by the emission efficiency at the emission wavelength (λ_{em}) because both the incoming and outgoing electric fields can be enhanced by SPRs.[28,29] The latter is actually related to the spontaneous emission rate at the emission wavelength. Therefore, the TPL of the GNR can be expressed as follows:[30]

dx.doi.org/10.1021/jp405403g | J. Phys. Chem. C 2013, 117, 20146−20153

$$I_{TPL} = \eta(\lambda_{em})\delta(\lambda_{ex})|E_0|^4 L^4(\lambda_{ex}) L^2(\lambda_{em}) \propto \eta(\lambda_{em})\delta(\lambda_{ex}) |E_0|^4 \left(\frac{1}{V}\int_{GNR} |E(\lambda_{ex}, r)/E_0|^4 \, dV\right) \left(\frac{1}{V}\int_{GNR} |E(\lambda_{em}, r)/E_0|^2 \, dV\right) \quad (2)$$

Here, $\eta(\lambda_{em})$ and $\delta(\lambda_{ex})$ are the quantum efficiency and TPA cross section of the GNR, V is the volume of the GNR, $E(\lambda_{ex}, r)$ and $E(\lambda_{em}, r)$ are the electric field distributions at the excitation and emission wavelengths, $L(\lambda_{ex}) = E(\lambda_{ex}, r)/E_0$ and $L(\lambda_{em}) = E(\lambda_{em}, r)/E_0$ denote the corresponding electric field enhancement factors, and E_0 is the electric field amplitude of the incident light. The integrals run over the volume of the GNR, and they represent the spatially averaged electric field enhancement factors at the excitation and emission wavelengths, respectively. Previously, the quantum efficiency of GNRs was measured to be $\sim 10^{-4}$–10^{-3}.[8]

So far, there are many experimental studies on the TPL of GNRs. It has been shown that the TPL of a GNR exhibits a strong dependence on the polarization of the excitation light. More concretely, the polarization-dependent TPL of a GNR generally exhibits the feature of a dipole that shows $\cos^4 \alpha$ dependence on the polarization angle α.[20]

In order to confirm the validity of eq 2, we have calculated the TPL of the GNR as a function of polarization angle by using λ_{ex} = 800 nm and λ_{em} = 550 nm. The result is shown in Figure 3 by empty circles. It can been seen clearly that the dependence of the TPL on the polarization angle follows a function of $\cos^4 \alpha$, which is given by the solid curve, implying that the relative TPL intensities of GNRs can be estimated by using eq 2. In fact, Wang et al. derived a similar formula to describe the TPL emitted by single GNRs.[30] What we have done here is to quantitatively introduce an spatially averaged enhancement factors at both the excitation and emission wavelengths by using the integral of the electric field inside the GNR. Ghenuche et al. used the distribution of $|E|^4$ to virtualize the spatial distribution of TPL in a nanoantenna formed by two coupled GNRs.[31] Very recently, Viarbitskaya et al. employed a similar method to calculate the TPL emitted by Au triangles.[32]

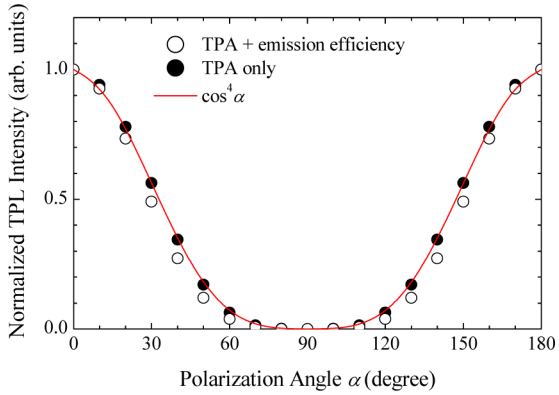

Figure 3. Polarization dependent TPL calculated by using eq 2 (open circles) and eq 4 (filled circles) for the GNR with a length of 45 nm and a diameter of 12 nm. The excitation and emission wavelengths are chosen to be 800 and 550 nm, respectively. The TPL intensity has been normalized to its maximum which appears at α = 0° and 180°. The solid curve shows a function of $\cos^4 \alpha$.

When the GNR-based sensor is used to detect an NP (or an NS), what we are concerned with is the modification of the TPL rather than its absolute intensity. When the NS is far from the GNR, its influence on the TPL of the GNR is negligible. Therefore, one can introduce a normalized TPL (I_{NOR}) by using the TPL of the system in which the NS is far from the GNR as reference to characterize the relative change in the TPL. It will be shown in the following that the information on the NS can be extracted from the normalized TPL, which can be defined as

$$I_{NOR}(s) = \frac{I_{GNR+NS}(s)}{I_{GNR+NS}(s \to \infty)} = \left[\left(\int_{GNR+NS} |E(\lambda_{ex}, r, s)/E_0|^4 \, dV\right) \left(\int_{GNR+NS} |E(\lambda_{em}, r, s)/E_0|^2 \, dV\right)\right] / \left[\left(\int_{GNR+NS} |E(\lambda_{ex}, r, s \to \infty)/E_0|^4 \, dV\right) \left(\int_{GNR+NS} |E(\lambda_{em}, r, s \to \infty)/E_0|^2 \, dV\right)\right] \quad (3)$$

Here, s is the distance between the NS and the GNR, which is defined as the gap between them. It can be seen that the quantum efficiency ($\eta(\lambda_{em})$) and TPA cross section ($\delta(\lambda_{ex})$) of the GNR, which are independent of s, have been canceled out in I_{NOR}. For the NSs studied in this paper, it can be seen later that the influence of the NS on the TPL of the GNR becomes negligible when the distance between them is larger than 50 nm. Therefore, we will use the TPL of the system with s = 50 nm as a reference for the normalization of the TPL. Since the TPL of the GNR (or GNR+NS) appears mainly in the visible light region, which is far from the LSPR of the GNR,[29] the influence of the NS on the electric field distribution at the emission wavelength ($E(\lambda_{em}, r)$) depends strongly on the material properties of the NS. It will be shown in the following that the enhancement at the emission wavelength needs to be taken into account for Au NSs whose SPRs appear in the visible light region. In comparison, this effect is not pronounced for Si NSs and can be neglected for SiO_2 NSs. Consequently, the normalized TPL for SiO_2 NSs can be further simplified as

$$I_{NOR}(s) = \frac{\left(\int_{GNR+NS} |E(\lambda_{ex}, r, s)/E_0|^4 \, dV\right)}{\left(\int_{GNR+NS} |E(\lambda_{ex}, r, s \to \infty)/E_0|^4 \, dV\right)} \quad (4)$$

Since the line width of the LSPR of the GNR is usually much larger than that of the femtosecond laser and the TPL scales quadraticlly with the intensity of the excitation light, the effect of the line width of the femtosecond laser on the TPL is not so pronounced. More importantly, we used a normalized TPL to sense NPs, and the effect of the femtosecond laser line width will be canceled out in the normalized TPL. Therefore, we did not consider the line width of the femtosecond laser in the numerical calculations.

3. RESULTS AND DISCUSSION

Dependence of TPL on Moving Direction and Particle Size. Let us first examine the modification of the normalized TPL of the system (GNR+NS) when Au NSs with different diameters (ϕ = 6, 12, and 24 nm) approach the GNR from different directions (θ = 0°, 30°, and 90°), as schematically

dx.doi.org/10.1021/jp405403g | J. Phys. Chem. C 2013, 117, 20146–20153

shown in Figure 1. The dependence of the TPL on the distance between the GNR and the NS is calculated for Au NSs with different sizes and moving directions. The excitation and detection wavelengths are chosen to be 800 and 550 nm, respectively. The results are presented in Figure 4.

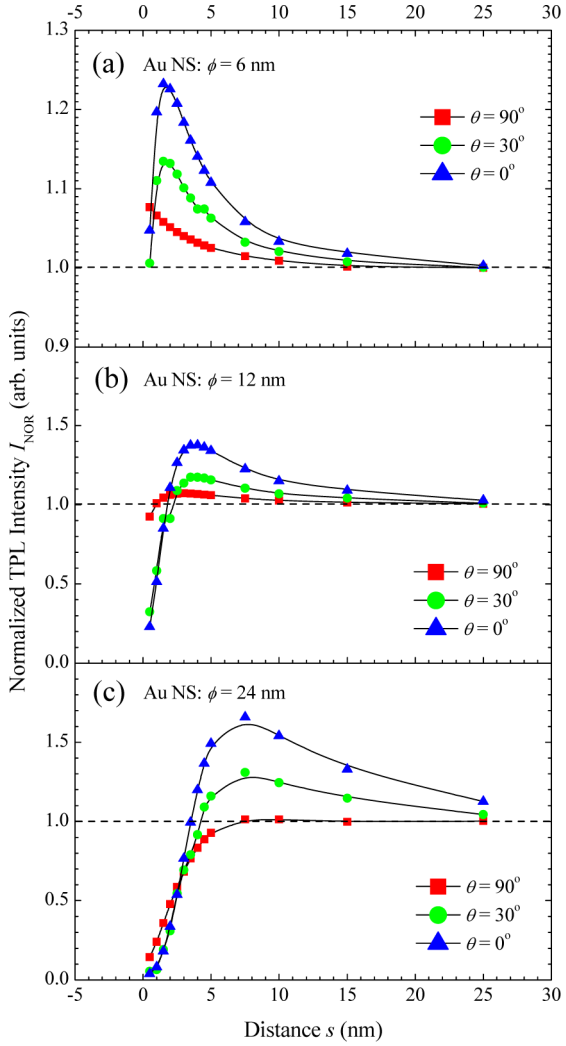

Figure 4. Evolution of the normalized TPL of the system (GNR+NS) when Au NSs with different diameters (ϕ = 6, 12, and 24 nm) approach the GNR from different directions (θ = 90°, 30°, and 0°).

For the moderate NS with ϕ = 12 nm, the evolution of I_{NOR} with decreasing s is found to depend strongly on the moving direction. When the moving direction is perpendicular to the long axis of the GNR (θ = 90°), I_{NOR} increases slightly with decreasing s, reaching its maximum of ~1.07 at s ~ 3 nm. After that, it begins to decrease to 0.92 at s = 0.5 nm. When the moving direction is changed to θ = 30°, a faster increase in I_{NOR} is observed for s > 3 nm where the maximum value of ~1.17 is achieved. In addition, a rapid decrease of I_{NOR} is found for s < 3 nm. It implies that I_{NOR} of the system is more sensitive to the NS coming from this direction. For the NS moving in the direction with θ = 0°, the maximum and minimum values of I_{NOR}, which are observed at s = 4 nm and s = 0.5 nm, are calculated to be ~1.38 and ~0.23, respectively. It indicates that I_{NOR} of the system is most sensitive to NSs moving in this direction.

In Figure 5, we present the distribution of $|E(\lambda_{ex}, r)/E_0|^4|E(\lambda_{em}, r)/E_0|^2$ (λ_{ex} = 800 nm, λ_{em} = 550 nm) on the xy plane

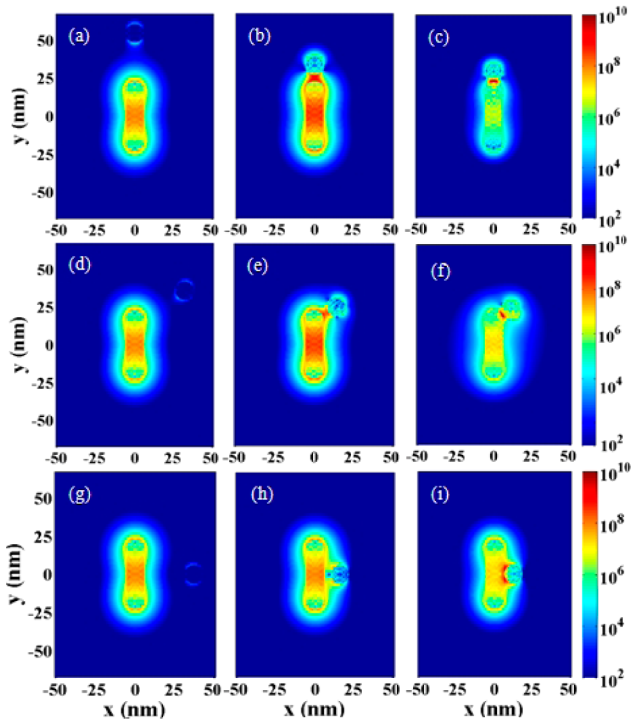

Figure 5. Evolution of $|E(\lambda_{ex}, r)/E_0|^4|E(\lambda_{em}, r)/E_0|^2$ (λ_{ex} = 800 nm, λ_{em} = 550 nm) distribution of the system on the xy plane when the Au NS with a diameter of 12 nm approaches the GNR from different directions (θ = 0°, 30°, and 90°). The distances between the GNR and the NS are chosen to be s = 25 nm (a,d,g), s = 4 nm (b,e,h), and s = 0.5 nm (c,f,i).

calculated for the system in which the Au NS with a diameter of ϕ = 12 nm appears at several specific positions (s = 0.5, 4, and 25 nm) in different moving directions. It can be seen that the electric field intensity in the GNR becomes stronger (i.e., the GNR becomes brighter) when the NS approaches the GNR from far places, especially for the direction with θ = 0°. However, the GNR becomes darker when the gap between the GNR and the NS is reduced to be smaller than 3 nm. A rapid and large reduction in the TPL of the GNR is also observed for the direction with θ = 30°. An interesting phenomenon observed in Figure 5 is the lightening of the NS when it reaches the vicinity of the GNR. Since the SPR of the NS is located at ~530 nm, the TPL from the NS is weak when it is excited at 800 nm because the absorption at this wavelength is quite small. When the NS moves to the vicinity of the GNR, the coupling between them is enhanced significantly, leading to the shift of the LSPR of the GNR. In the case, we should treat them as a system and consider the NS as part of the GNR. As a result, the NS is lightened and becomes brighter.

In the numerical calculation, we can easily extract the contribution of the NS to the total TPL of the system, which is also a function of s. It is shown in Figure 6. We can see that the TPL of the NS increases monotonically with decreasing distance. It means that the NS becomes brighter when it approaches the GNR, confirming the lightening of the NS discussed above. This effect contributes positively to the total TPL for s > 4 nm and negatively for s < 4 nm from the viewpoint of sensing.

dx.doi.org/10.1021/jp405403g | J. Phys. Chem. C 2013, 117, 20146−20153

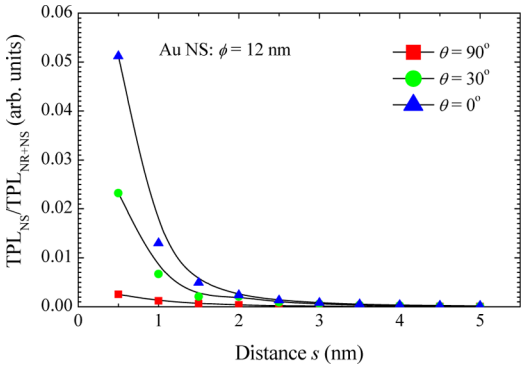

Figure 6. Contribution of the Au NS with a diameter of 12 nm to the total TPL of the system (GNR+NS) when it approaches the GNR from different directions (θ = 90°, 30°, and 0°).

In order to gain a deep insight into the physical mechanism responsible for the modification of the TPL, we calculated the absorption spectra of the system for different values of s, as shown in Figure 7a. It can be seen that for s = 25 nm, the coupling between the GNR and the NS is negligible, and the absorption of the system is the same as that of the GNR. When s is reduced to 10 nm, a redshift of the absorption peak as well as an increase of the peak value is observed. As a result, the absorption at the excitation wavelength (λ_{ex} = 800 nm) is increased, leading to the increase in the TPL of the system. A further increase in peak absorption is found for s = 7.5, 5.0, and 4.0 nm. The situation is changed when s is reduced to be 3.0 nm. In this case, the large redshift of the peak wavelength results in a reduction of the absorption at the excitation wavelength. Consequently, the TPL begins to decrease at this distance. After that, the redshift of the absorption peak becomes significant, while the increase in the peak absorption gradually saturates. For this reason, the absorption at the excitation wavelength decreases rapidly, leading to the significant reduction in the TPL of the system. The maximum peak absorption is observed at s = 1.5 nm. After that, one can see a decrease of the peak absorption and a broadening of the absorption spectrum.

So far, we have discussed in detail the evolution of the TPL of the system when a NS with ϕ = 12 nm approaches the GNR from different directions, which is shown in Figure 4b. When the diameter of the NS is reduced to 6 nm or increased to 24 nm, the nonlinear optical response of the GNR is completely different, as shown in Figure 4a,c. For the small NS, I_{NOR} is observed to increase with decreasing s for all moving directions. For θ = 0° and 30°, it begins to decrease after reaching maximum values of about 1.23 and 1.13 at s = 1.5 nm. However, the TPL is still larger than 1.0 even at the smallest distance of s = 0.5 nm. This behavior is completely different from that observed for the moderate NS shown in Figure 4b, where the I_{NOR} is only ~0.23−0.33 at s = 0.5 nm. For θ = 90°, a monotonic increase in I_{NOR} is observed with decreasing s. This feature enables us to easily discriminate small NSs from large ones, and it originates from the slightly detuning of the excitation wavelength (800 nm) from the LSPR of the GNR (795 nm). For the large NS, the evolution of the TPL is quite similar to that observed for the moderate NS. However, the minimum I_{NOR} observed at s = 0.5 nm is quite small for all moving directions. In addition, the maximum I_{NOR} observed for θ = 0° reaches ~1.66 at a large distance of s = 7.5 nm. For θ = 90°, the I_{NOR} begins to decrease at s = 10 nm. All these

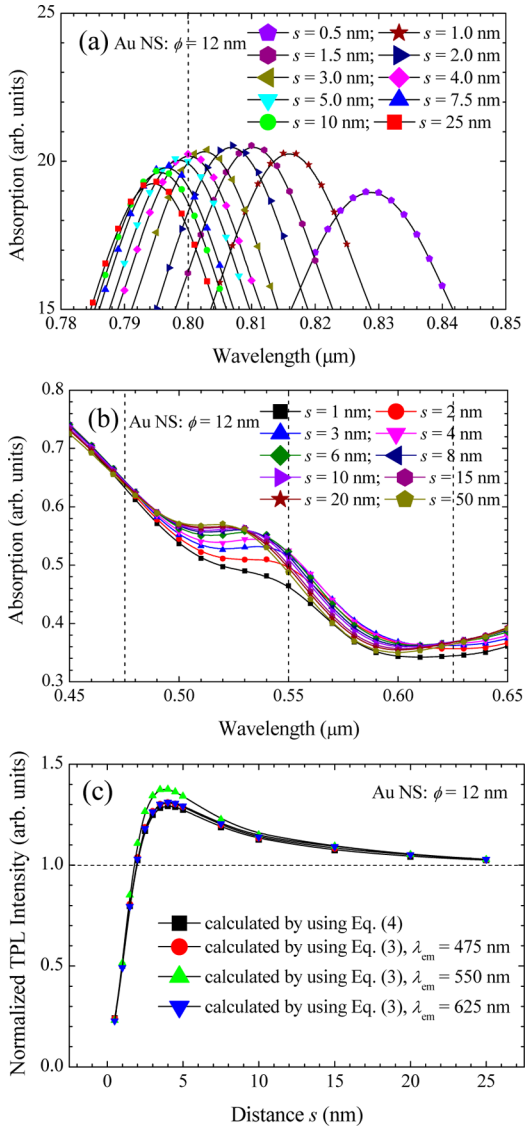

Figure 7. Evolution of the absorption spectrum of the system (GNR + NS) in the spectral range of 0.78−0.85 μm (a) and of 0.45−0.65 μm (b) when the Au NS (ϕ = 12 nm) approaches the GNR from far place along the direction with θ = 0°. The dependences of the normalized TPL on the distance calculated by using eq 2 for different detecting wavelengths and by using eq 4 are compared in panel c.

behaviors indicate that the large NS starts to influence the TPL of the GNR at a much longer distance. In other words, it is easier to detect large NPs.

In order to see the influence of the emission efficiency on the TPL, we calculated the evolution of the absorption spectrum in the visible spectral region (450−650 nm) with increasing distance between the Au NS (ϕ = 12 nm) and the GNR, as shown in Figure7b. It can be seen clearly that the change in absorption, which implies a modification in the electric field inside the GNR and NS, occurs mainly at the SPR of the Au NS (530 nm). If we choose to detect the TPL at this wavelength, the modification in the emission efficiency in the TPL has to be taken into account. In comparison, the change in the emission efficiency of the TPL can be neglected for a detection wavelength far from the SPR of the Au NS. In Figure 7c, we compare the evolution of I_{NOR} of the system calculated for three different detection wavelengths (475, 550, and 625 nm).

dx.doi.org/10.1021/jp405403g | J. Phys. Chem. C 2013, 117, 20146−20153

It can be seen that the evolution of I_{NOR} appears to be similar for λ_{em} = 475 and 625 nm. For λ_{em} = 550 nm, the maximum TPL appears to be larger due to the pronounced lightening effect of the Au NS at its SPR.

In practice, one can detect the TPL in a broad wavelength range or at a specific wavelength. When the polarization-dependent TPL of a GNR is measured, we usually choose to detect the TPL of the GNR in a broad wavelength range in order to enhance the signal-to-noise ratio. In this case, we need to consider an averaged emission efficiency over a broad wavelength range for the TPL. As a result, the influence of the polarization on the emission efficiency may become negligible. In Figure3, we also present the calculated polarization-dependent TPL of the GNR by using eq 4 in which only the TPA cross section is taken into account, as shown by the solid circles. It can be seen that the polarization-dependent TPL without considering the emission efficiency follows exactly a function of $\cos^4 \alpha$, implying that the effect of emission efficiency has been smeared out when the average over a broad wavelength range is taken into account. For the GNR-based sensor studied in this paper, the detection of the normalized TPL at a specific wavelength is preferred for Au NSs because the sensitivity can be further enhanced by exploiting the lightening effect of the Au NSs at their SPRs.

In practice, one can choose to detect the modification in the linear (e.g., absorption or scattering) or nonlinear optical signals (e.g., TPL) of the GNR induced by NSs. In order to show the higher sensitivity offered by detecting the nonlinear optical properties of the GNR, we compare the dependences of the normalized absorption, scattering, and TPL intensities on the distance between the Au NS (ϕ = 12 nm) and the GNR, as shown in Figure 8. It is apparent that the maximum TPL

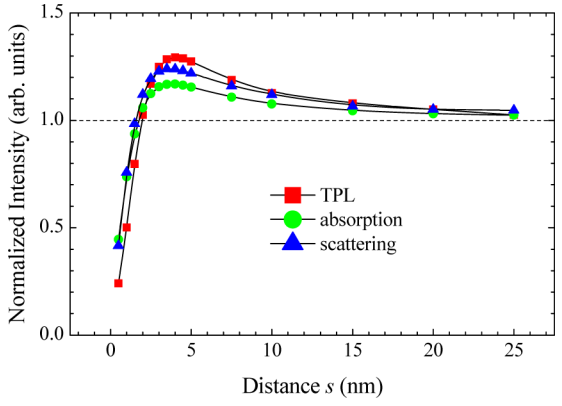

Figure 8. Comparison of the sensitivities of the GNR-based sensor for detecting linear and nonlinear optical signals. The dependences of TPL, absorption, and scattering intensities on the distance between the Au NS (ϕ = 12 nm) and the GNR are presented.

intensity is larger than those of the absorption and scattering, and it appears at a larger distance. In addition, the minimum TPL intensity is also smaller than those of the absorption and scattering, implying that a higher sensitivity can be achieved by detecting TPL.

Dependence of TPL on Particle Material. Apart from the moving direction and size of NSs, the TPL-based sensor proposed here can also discriminate particle material. In Figure 9, we present the calculation results for Si NSs with three different diameters of ϕ = 6, 12, and 24 nm. The dispersion in the refractive index of Si was considered, and its refractive

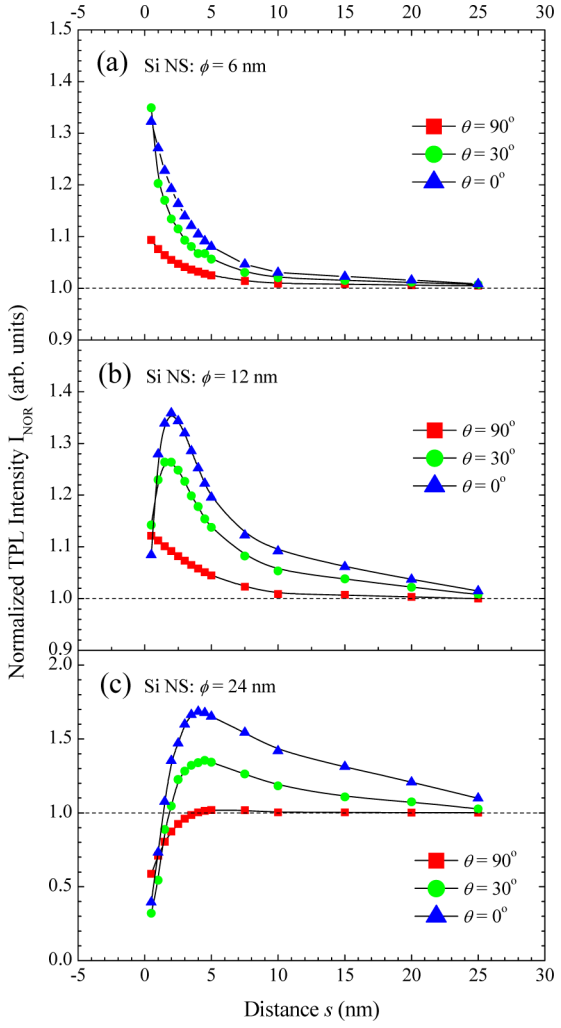

Figure 9. Evolution of the normalized TPL of the system (GNR+NS) when Si NSs with different diameters (ϕ = 6, 12, and 24 nm) approach the GNR from different directions (θ = 90°, 30°, and 0°).

indexes at 800 and 550 nm were chosen to be 3.681 + 0.005 i and 4.077 + 0.028 i, respectively.[26] For the NS with ϕ = 6 nm, a monotonic increase in I_{NOR} is observed for all moving directions. The maximum I_{NOR}, which is about 1.35, is observed at s = 0.5 nm for θ = 30°. For the NS with moderate size, a decrease in I_{NOR} is found for θ = 0° and 30° when the distance becomes smaller than 2.0 nm. However, the I_{NOR} at the smallest distance of 0.5 nm is still larger than 1.0 for both cases. This behavior is quite similar to the Au NS with ϕ = 6 nm. For the Si NS with ϕ = 24 nm, the evolution of the I_{NOR} with decreasing distance is quite similar to that observed for the Au NS with the same size because of the large refractive index of Si.

In Figure 10, we present the calculation results for SiO_2 NSs with three different diameters (ϕ = 6, 12, and 24 nm). Similarly, the dispersion in the refractive index of SiO_2 was taken into account, and its refractive indexes at 800 and 550 nm were chosen to be 1.4533 and 1.4599, respectively.[26] In all cases, we observe a monotonic increase in I_{NOR}. However, the maximum I_{NOR}, which is found at s = 0.5 nm, increases with increasing diameter of NSs. For the NS with ϕ = 6 nm, the maximum I_{NOR} is only 1.03. It increases to about 1.16 for the NS with ϕ = 24 nm.

The different responses of the GNR to the approaching NSs made of different materials (metal, semiconductor, and

dx.doi.org/10.1021/jp405403g | J. Phys. Chem. C 2013, 117, 20146−20153

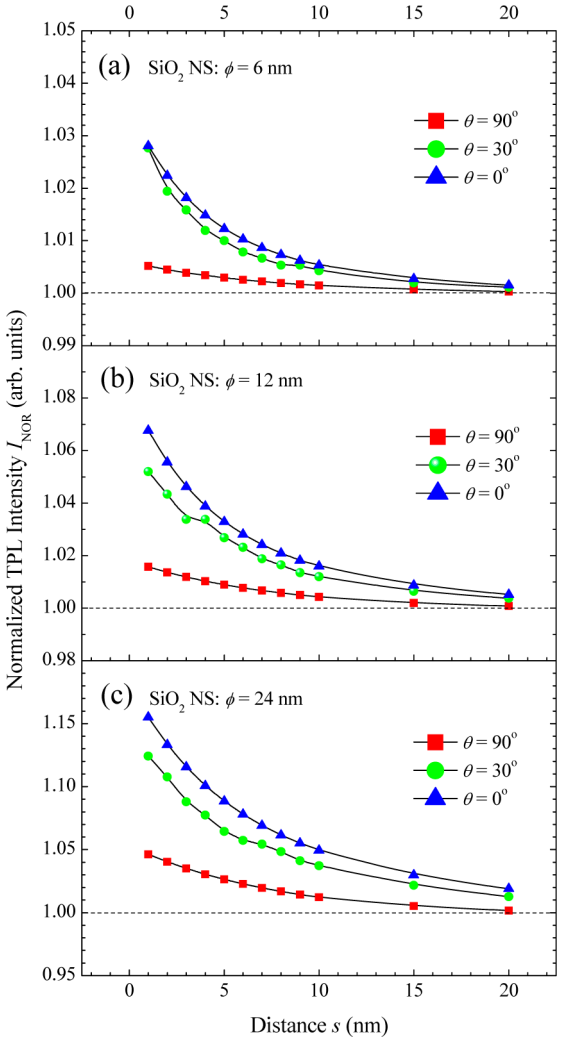

Figure 10. Evolution of the normalized TPL of the system (GNR +NS) when SiO_2 NSs with different diameters (ϕ = 6, 12, and 24 nm) approach the GNR from different directions (θ = 90°, 30°, and 0°).

dielectric) shown in Figures 4, 9, and 10, which are manifested in the modification of the TPL, enable us to discriminate particle material. However, the determination of particle material usually needs other information about NPs such as their sizes and locations, and the later information is not easy to be obtained in practice. From Figures 4, 9, and 10, one can easily find the advantage of choosing an excitation wavelength, which is slightly detuned from the LSPR of the GNR. The normalized TPL of the system remains larger than 1.0 for all small NSs with ϕ = 6 nm, implying that one can easily discriminate small NPs from large ones based on this feature.

Dependence of Response and Sensitivity on the Size of GNR. The sensitivity of the sensor proposed here depends strongly on the size of the GNR. Here, we compare the performance of the sensor discussed above with that of a smaller sensor whose length (23 nm) and diameter (6 nm) are only half of those of the GNR. Since a redshift in LSPR is found for GNRs with increasing volume when the aspect ratio is fixed,[33] the aspect ratio of the small GNR is slightly increased from 3.75 to 3.83 so that its LSPR still appears at 795 nm. In Figure 11, we compare the response behaviors of the two sensors in the sensing of an Au NS with ϕ = 12 nm and θ = 0°. Although the evolution of I_{NOR} for the two sensors with

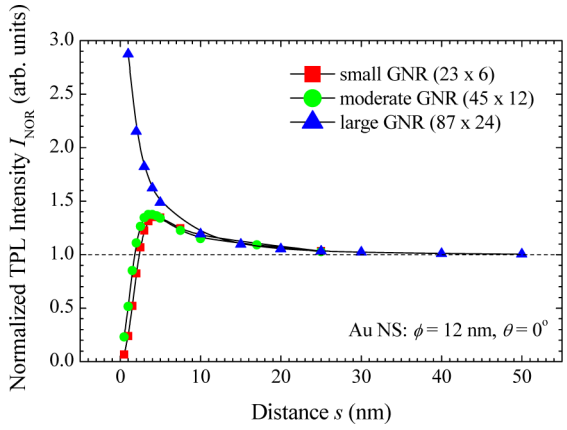

Figure 11. Comparison of the response and sensitivity of the sensors built with small, moderate and large GNRs. An Au NS with ϕ = 12 nm and θ = 0° is used as a probe.

decreasing distance appears to be similar, a detailed inspection reveals that the sensor based on the small GNR possesses higher sensitivity as compared to that built with the moderate GNR. In Figure 11, it can be seen that the maximum changes in I_{NOR} achieved by the two sensors are almost the same. However, the small sensor reaches its maximum I_{NOR} at s = 4.5 nm, while the moderate one reaches its maximum I_{NOR} at a smaller distance of s = 3.5 nm. In addition, the minimum I_{NOR} observed for the small sensor is 0.07, while that observed for the moderate one is 0.23. These two features clearly indicate that the small sensor possesses higher sensitivity as compared to the moderate one. There are two possible reasons that are responsible for the higher sensitivity achieved by the small sensor. For the small GNR, the extinction is completely dominated by absorption and scattering is almost negligible. With increasing size, scattering becomes more and more important, and it begins to influence TPA process because the electric field inside the GNR and thus the absorption becomes weaker. On the other hand, the sensitivity is thought to depend on the relative volume of the sensor with respect to the NP being detected. The sensitivity is high when the volume of the sensor is comparable to or smaller than the NP.

In Figure 11, we also present the calculation results for a large GNR with a length of 87 nm and a diameter of 24 nm. Its LSPR is also located at 795 nm by slightly decreasing the aspect ratio from 3.75 to 3.63. It can be seen that the I_{NOR} increases monotonically when the Au NS approaches the GNR from a far place. A rapid increase in the I_{NOR} is observed for s < 10 nm and the maximum I_{NOR} reaches ~3.0 at the smallest distance of s = 0.5 nm. The nonlinear optical response of the large GNR is completely different from those observed for the moderate and small GNRs. It is because that the size of the Au NS is much smaller than that of the GNR and its influence to the TPL is positively even at a small distance of s = 0.5 nm. Therefore, various information on a NP can be extracted by arranging several GNRs with different sizes on the moving path of the NP.

4. CONCLUSIONS

In summary, we have proposed a simple numerical method to evaluate the TPL emitted by a GNR and systematically investigated the modification in the TPL of the system when an NS approaches the GNR from far place. It was found that the change in the TPL is sensitive to the size, material, and moving

dx.doi.org/10.1021/jp405403g | J. Phys. Chem. C 2013, 117, 20146−20153

direction of the NS. Consequently, the evolution of the TPL of the system exhibits different response behaviors when NSs of different sizes and materials approach the GNR from different directions. It was also revealed that the sensitivity and response of the GNR-based sensors depend strongly on their sizes. The results presented in this work clearly indicates that the nonlinear optical properties of GNRs, such as TPL studied in this paper, are more sensitive to the change in the environment surrounding the GNRs than their linear optical properties. Therefore, sensors with high sensitivity and multiple functions can be realized by monitoring the change in the nonlinear optical signals of the GNRs.

AUTHOR INFORMATION

Corresponding Author

*E-mail: slan@scnu.edu.cn; fax: +86-20-39310309.

Notes

The authors declare no competing financial interest.

ACKNOWLEDGMENTS

The authors acknowledge the financial support from the National Natural Science Foundation of China (Grant No. 51171066), the Ministry of Education of China (Grant No. 20114407110002), and the project for high-level professionals in the universities of Guangdong province, China.

REFERENCES

(1) Prasad, P. N. *Nanophotonics*; John Wiley & Sons, Inc.: New York, 2004.

(2) Nie, S.; Emory, S. R. Probing Single Molecules and Single Nanoparticles by Surface-Enhanced Raman Scattering. *Science* **1997**, *275*, 1102−1106.

(3) Huang, X.; El-Sayed, I. H.; Qian, W.; El-Sayed, M. A. Cancer Cells Assemble and Align Gold Nanorods Conjugated to Antibodies to Produce Highly Enhanced, Sharp, and Polarized Surface Raman Spectra: A Potential Cancer Diagnostic Marker. *Nano Lett.* **2007**, *7*, 1591−1597.

(4) Qian, X.; Peng, X.; Ansari, D. O.; Yin-Goen, Q.; Chen, G. Z.; Shin, D. M.; Yang, L.; Young, A. N.; Wang, M. D.; Nie, S. In Vivo Tumor Targeting and Spectroscopic Detection with Surface-Enhanced Raman Nanoparticle Tags. *Nat. Biotechnol.* **2008**, *26*, 83−90.

(5) Chon, J. W. M.; Bullen, C.; Zijlstra, P.; Gu, M. Spectral Encoding on Gold Nanorods Doped in a Silica Sol−Gel Matrix and Its Application to High-Density Optical Data Storage. *Adv. Funct. Mater.* **2007**, *17*, 875−880.

(6) Zijlstra, P.; Chon, J. W. M.; Gu, M. Five-Dimensional Optical Recording Mediated by Surface Plasmons in Gold Nanorods. *Nature* **2009**, *459*, 410−413.

(7) Li, X.; Lan, T. H.; Tien, C. H.; Gu, M. Three-Dimensional Orientation-Unlimited Polarization Encryption by a Single Optically Configured Vectorial Beam. *Nat. Commun.* **2012**, *3*, 998.

(8) Mohamed, M. B.; Volkov, V.; Link, S.; El-Sayed, M. A. The 'Lightning' Gold Nanorods: Fluorescence Enhancement of Over a Million Compared to The Gold Metal. *Chem. Phys. Lett.* **2000**, *317*, 517−523.

(9) Nikoobakht, B.; El-Sayed, M. A. Preparation and Growth Mechanism of Gold Nanorods (NRs) Using Seed-Mediated Growth Method. *Chem. Mater.* **2003**, *15*, 1957−1962.

(10) Grzelczak, M.; Pérez-Juste, J.; Mulvaney, P.; Liz-Marzán, L. M. Shape Control in Gold Nanoparticle Synthesis. *Chem. Soc. Rev.* **2008**, *37*, 1783−1791.

(11) Gu, F. X.; Zhang, L.; Yin, X. F.; Tong, L. M. Polymer Single-Nanowire Optical Sensors. *Nano Lett.* **2008**, *8*, 2757−2761.

(12) Lu, G.; Hou, L.; Zhang, T.; Li, W.; Liu, J.; Perriat, P.; Gong, Q. Anisotropic Plasmonic Sensing of Individual or Coupled Gold Nanorods. *J. Phys. Chem. C* **2011**, *115*, 22877−22885.

(13) Zijlstra, P.; Paulo, P. M. R.; Orrit, M. Optical Detection of Single Non-absorbing Molecules Using the Surface Plasmon Resonance of a Gold Nanorod. *Nat. Nanotechnol.* **2012**, *7*, 379−382.

(14) Shao, L.; Fang, C.; Chen, H.; Man, Y. C.; Wang, J.; Lin, H. Q. Distinct Plasmonic Manifestation on Gold Nanorods Induced by the Spatial Perturbation of Small Gold Nanospheres. *Nano Lett.* **2012**, *12*, 1424−1430.

(15) Bouhelier, A.; Bachelot, R.; Lerondel, G.; Kostcheev, S.; Royer, P.; Wiederrecht, G. P. Surface Plasmon Characteristics of Tunable Photoluminescence in Single Gold Nanorods. *Phys. Rev. Lett.* **2005**, *95*, 267405.

(16) Qiu, L.; Larson, T. A.; Smith, D.; Vitkin, E.; Modell, M. D. Observation of Plasmon Line Broadening in Single Gold Nanorods. *Appl. Phys. Lett.* **2008**, *93*, 153106.

(17) Liu, M.; Pelton, M.; Guyot-Sionnest, P. Reduced Damping of Surface Plasmons at Low Temperatures. *Phys. Rev. B* **2009**, *79*, 035418.

(18) Hayakawa, T. B.; Usui, Y.; Bharathi, S.; Nogami, M. Second Harmonic Generation from Coupled Surface-Plasmon Resonances in Self-Assembled Gold-Nanoparticle Monolayers Coated with an Aminosilane. *Adv. Mater.* **2004**, *16*, 1408−1412.

(19) Czaplicki, R.; Husu, H.; Siikanen, R.; Makitalo, J.; Kauranen, M. Enhancement of Second-Harmonic Generation from Metal Nanoparticles by Passive Elements. *Phys. Rev. Lett.* **2013**, *110*, 093902.

(20) Wang, H.; Huff, T. B.; Zweifel, D. A.; He, W.; Low, P. S.; Wei, A.; Cheng, J. In Vitro and In Vivo Two-Photon Luminescence Imaging of Single Gold Nanorods. *Proc. Natl. Acad. Sci. U.S.A.* **2005**, *102*, 15752−15756.

(21) Farrer, R. A.; Butterfield, F. L.; Chen, V. W.; Fourkas, J. T. Highly Efficient Multiphoton-Absorption-Induced Luminescence from Gold Nanoparticles. *Nano Lett.* **2005**, *5*, 1139−1142.

(22) Lippitz, M.; Dijk, M. A.; Orrit, M. Third-Harmonic Generation from Single Gold Nanoparticles. *Nano Lett.* **2005**, *5*, 799−802.

(23) Deng, H.; Li, G.; Dai, Q.; Ouyang, M.; Lan, S.; Trofimov, V. A.; Lysak, T. M. Size Dependent Competition between Second Harmonic Generation and Two-Photon Luminescence Observed in Gold Nanoparticles. *Nanotechnology* **2013**, *24*, 075201.

(24) Yurkin, M. A.; Maltsev, V. P.; Hoekstra, A. G. The Discrete Dipole Approximation: An Overview and Recent Developments. *J. Quant. Spectrosc. Radiat. Transfer* **2007**, *106*, 546−557.

(25) Draine, B. T.; Flatau, P. J. User Guide to the Discrete Dipole Approximation Code DDSCAT 7.0. *arXiv.org, e-Print Arch., Astrophys.* **2009**, No. arXiv:0809.0337v5.

(26) The information on the refractive indices of materials is available on the website http://refractiveindex.info/

(27) Xu, C.; Webb, W. W. Measurement of Two-Photon Excitation Cross Sections of Molecular Fluorophores with Data from 690 to 1050 Nm. *J. Opt. Soc. Am. B* **1996**, *13*, 481−491.

(28) Boyd, G. T.; Rasing, T.; Leite, J. R. R.; Shen, Y. R. Local-Field Enhancement on Rough Surfaces of Metals, Semimetals, and Semiconductors with the Use of Optical Second-Harmonic Generation. *Phys. Rev. B* **1984**, *30*, 519−526.

(29) Boyd, G. T.; Yu, Z. H.; Shen, Y. R. Photoinduced Luminescence from The Noble Metals and Its Enhancement on Roughened Surfaces. *Phys. Rev. B* **1986**, *33*, 7923−7936.

(30) Wang, D.; Hsu, F.; Lin, C. Surface Plasmon Effects on Two Photon Luminescence of Gold Nanorods. *Opt. Express* **2009**, *17*, 11350−11359.

(31) Ghenuche, P.; Cherukulappurath, S.; Taminiau, T. H.; Hulst, N. F.; Quidant, R. Spectroscopic Mode Mapping of Resonant Plasmon Nanoantennas. *Phys. Rev. Lett.* **2008**, *101*, 116805.

(32) Viarbitskaya, S.; Teulle, A.; Marty, R.; Sharma, J.; Girard, C.; Arbouet, A.; Dujardin, E. Tailoring and Imaging the Plasmonic Local Density of States in Crystalline Nanoprisms. *Nat. Mater.* **2013**, *12*, 426−432.

(33) Prescoot, S. W.; Mulvaney, P. Gold Nanorod Extinction Spectra. *J. Appl. Phys.* **2006**, *99*, 123504.